

FORWARD PHYSICS AT THE LHC:  
FROM THE STRUCTURE OF THE POMERON  
TO THE SEARCH FOR  $\gamma$ -INDUCED RESONANCES

CHRISTOPHE ROYON

The University of Kansas, Lawrence, USA  
christophe.royon@ku.edu

*(Received June 2, 2016)*

*Dedicated to Andrzej Bialas in honour of his 80th birthday*

We describe some of the future measurements to be performed by the CMS, TOTEM and ATLAS collaborations on hard diffraction in order to understand better the structure of the Pomeron. We also describe the prospects concerning the search for quartic  $\gamma\gamma\gamma\gamma$  anomalous couplings and discuss a possible interpretation for the existence of a new particle decaying into two photons at a mass of about 750 GeV.

DOI:10.5506/APhysPolB.47.1781

In this short review, we will describe some potential measurements to be performed at the LHC mainly in the ATLAS, CMS-TOTEM, CT-PPS experiments in order to get a better understanding of diffraction and photon-exchange processes. Of special interest will be the discussion of beyond Standard Model reaches, especially in the di-photon channel that might be the first sign of new physics. These studies follow a long-term collaboration with Prof. Andrzej Bialas and Prof. Robert Peschanski, that started after my Ph.D. in Saclay, about the dipole model and diffraction [1] and I would like to express all my gratitude to Andrzej for this long-term and successful collaboration, and to wish him a very nice birthday for this occasion.

**1. Experimental definition of diffraction and measurement  
of the gluon density in the Pomeron at HERA**

In this section, we discuss the different experimental ways to define diffraction. As an example, we describe the methods used by the H1 and ZEUS experiments at HERA, DESY, Hamburg in Germany since it is the

starting point for any diffraction studies at the LHC (most of the quark and gluon densities in the Pomeron were obtained using HERA data). In addition, many results concerning diffraction have been obtained at the Tevatron and the LHC will allow to extend these measurements in a completely new kinematical domain.

### 1.1. The rapidity gap method

HERA is a collider where electrons of 27.6 GeV collide with protons of 920 GeV. A typical event, as shown in the upper plot of Fig. 1, is  $ep \rightarrow eX$  where electron and jets are produced in the final state. We notice that the electron is scattered in the H1 backward detector<sup>1</sup> (in light grey/green) whereas some hadronic activity is present in the forward region of the detector (in the LAr calorimeter and in the forward muon detectors). The proton is thus completely destroyed and the interaction leads to jets and proton remnants directly observable in the detector. The fact that much energy is observed in the forward region is due to colour exchange between the scattered jet and the proton remnants. In about 10% of the events, the situation is completely different. Such events appear like the one shown in the bottom plot of Fig. 1. The electron is still present in the backward detector, there is still some hadronic activity (jets) in the LAr calorimeter, but no energy above noise level is deposited in the forward part of the LAr calorimeter or in the forward muon detectors. In other words, there is no colour exchange between the proton and the produced jets. As an example, this can be explained if the proton stays intact after the interaction.

This experimental observation leads to the first definition of diffraction: request a rapidity gap (in other words, a domain in the forward detectors where no energy is deposited above noise level) in the forward region. For example, the H1 Collaboration requests no energy deposition in the rapidity region  $3.3 < \eta < 7.5$ , where  $\eta$  is the pseudorapidity. Let us note that this approach does not insure that the proton stays intact after the interaction, but it represents a limit on the mass of the produced object  $M_Y < 1.6$  GeV. Within this limit, the proton could be dissociated. The advantage of the rapidity gap method is that it is quite easy to implement and it has a large acceptance in the diffractive kinematical plane. The inconvenience is that it is difficult to use at the LHC because of pile-up events. In order to accumulate high luminosities at the LHC, many proton interactions occur within the same bunch crossing and a diffractive event will be overlapping with non-diffractive events that will induce the presence of energy in the forward region.

---

<sup>1</sup> At HERA, the backward (resp. forward) directions are defined as the direction of the outgoing electron (resp. proton).

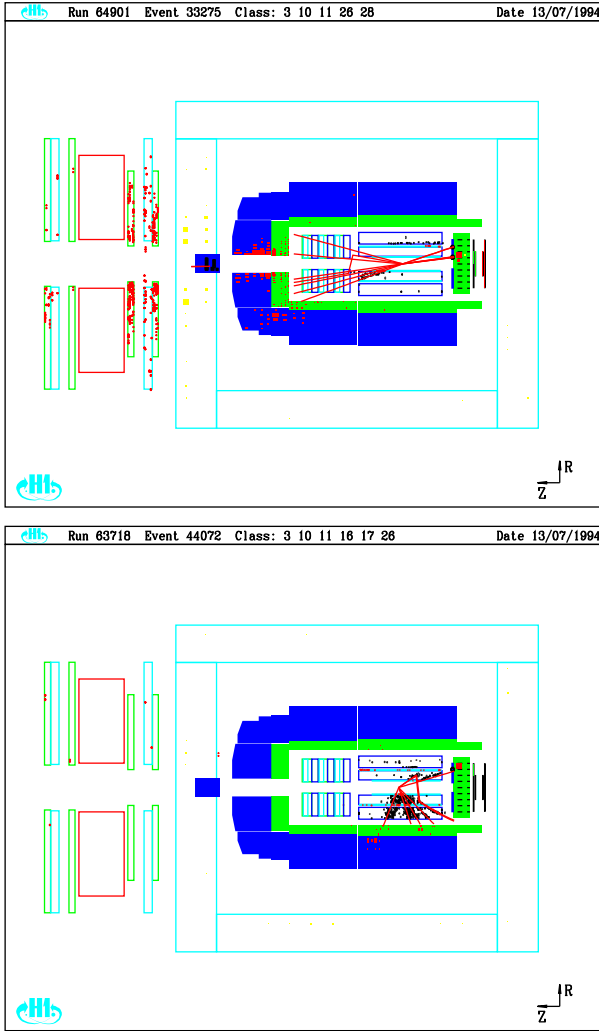


Fig. 1. “Usual” and diffractive events in the H1 experiment.

### 1.2. Proton tagging

The second experimental method to detect diffractive events is also natural: the idea is to detect directly the intact proton in the final state. The proton loses a small fraction of its energy and is thus scattered at very small angle with respect to the beam direction. Some special detectors called Roman Pots can be used to detect the protons close to the beam. The basic idea is simple: the Roman Pot detectors are located far away from the interaction point and can move close to the beam, when the beam is stable, to

detect protons scattered at vary small angles. The inconvenience is that the kinematical reach of those detectors is usually smaller than with the rapidity gap method. On the other hand, the advantage is that it gives a clear signal of diffraction since it measures the diffracted proton directly.

A scheme of a Roman Pot detector as it is used by the H1 or ZEUS experiment is shown in Fig. 2, and similar detectors are used by the TOTEM, CMS-TOTEM and ATLAS collaborations at the LHC. The beam is the horizontal line at the upper part of the figure. The detector is located in the pot itself and can move closer to the beam when the beam is stable enough (during the injection period, the detectors are protected in the home position). Step motors allow to move the detectors with high precision. A precise knowledge of the detector position is necessary to reconstruct the transverse momentum of the scattered proton and thus the diffractive kinematical variables. The detectors are placed in a secondary vacuum with respect to the beam one.

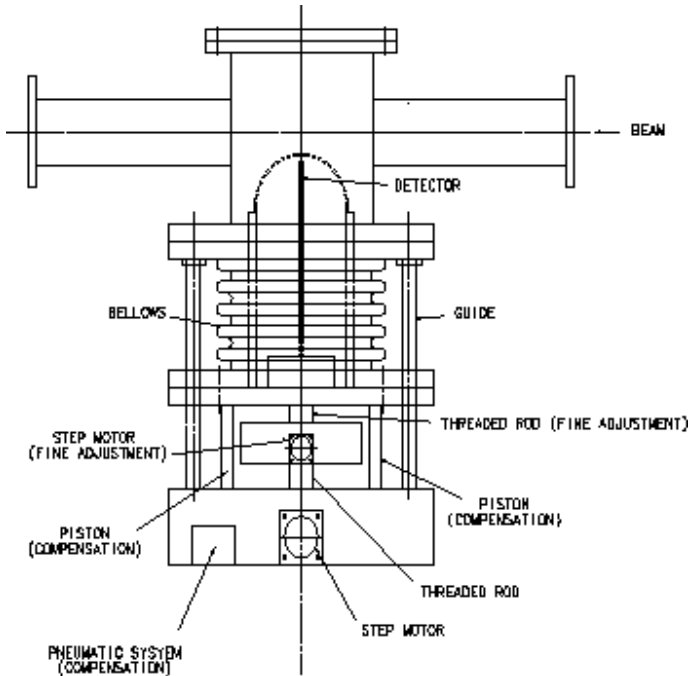


Fig. 2. Scheme of a Roman Pot detector.

1.3. Diffractive kinematical variables

After having described the different experimental definitions of diffraction at HERA, we will give the new kinematical variables used to characterise diffraction. A typical diffractive event is shown in Fig. 3, where  $ep \rightarrow epX$  is depicted. In addition to the usual deep inelastic variables,  $Q^2$  — the transferred energy squared at the electron vertex,  $x$  — the fraction of the proton momentum carried by the struck quark,  $W^2 = Q^2(1/x - 1)$  — the total energy in the final state, new diffractive variables are defined:  $x_P$  (called  $\xi$  at the Tevatron and the LHC) is the momentum fraction of the proton carried by the colourless object called the Pomeron, and  $\beta$  — the momentum fraction of the Pomeron carried by the interacting parton inside the Pomeron, if we assume the Pomeron to be made of quarks and gluons

$$x_P = \xi = \frac{Q^2 + M_X^2}{Q^2 + W^2}, \tag{1}$$

$$\beta = \frac{Q^2}{Q^2 + M_X^2} = \frac{x}{x_P}. \tag{2}$$

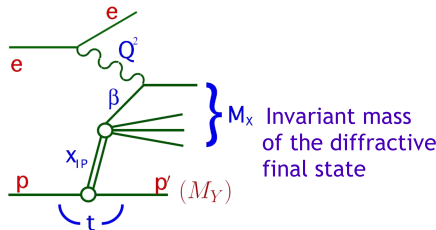


Fig. 3. Scheme of a diffractive event at HERA.

1.4. Extraction of the gluon density in the Pomeron

The general idea is to measure the cross section to produce diffractive events either by requesting the presence of a rapidity gap in the forward direction or of a tagged proton in Roman Pot detectors as a function of the  $t, \xi, \beta, Q^2$  kinematic variables. The following step is to perform Dokshitzer–Gribov–Lipatov–Altarelli–Parisi (DGLAP) [2] fits to the Pomeron structure function. If we assume that the Pomeron is made of quarks and gluons, it is natural to check whether the DGLAP evolution equations are able to describe the  $Q^2$  evolution of these parton densities.

The DGLAP QCD fit allows to get the parton distributions in the Pomeron as a direct output of the fit [3], and they are displayed in Fig. 4 as a blue shaded area as a function of  $\beta$ . We first note that the gluon density is

much higher than the quark one, showing that the Pomeron is gluon dominated. We also note that the gluon density at high  $\beta$  is poorly constrained which is shown by the larger shaded area. The measurement of di-jet cross section in diffraction allows constraining the gluon density further but the high  $\beta$  density is still poorly constrained.

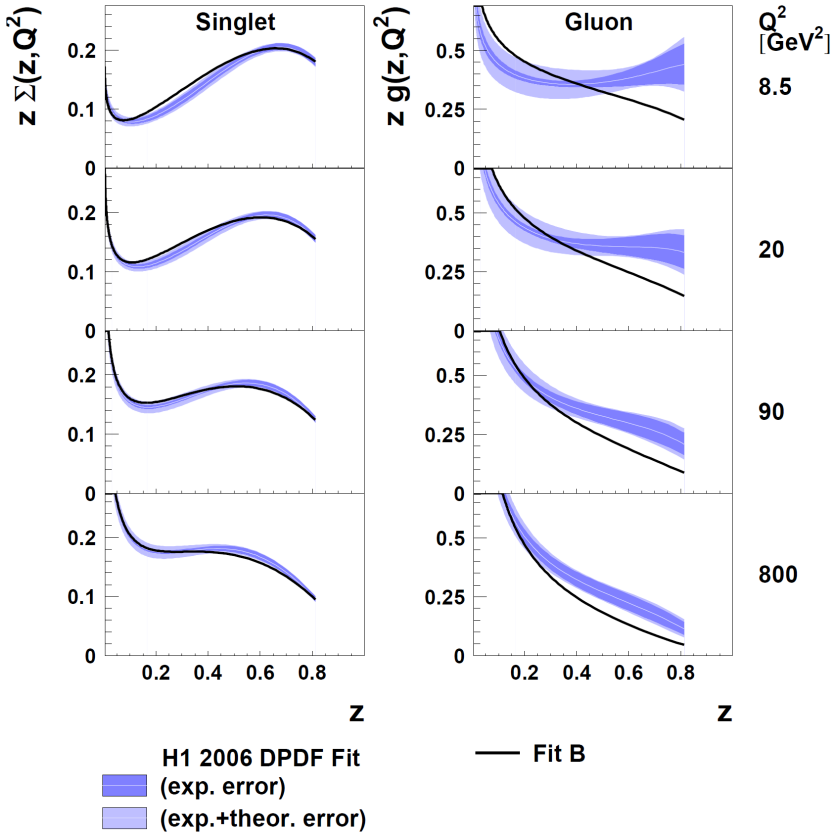


Fig. 4. Extraction of the parton densities in the Pomeron using a DGLAP NLO fit [H1 Collaboration].

## 2. Diffraction at the LHC

In the same way that we discuss diffraction at HERA, diffraction can occur at the LHC, the 13 TeV  $pp$  collider located close to Geneva, at CERN, Switzerland. In that case, one can have diffraction on one side only (single diffraction) or on both sides (double Pomeron exchange).

### 2.1. Diffractive kinematical variables

As we just mentioned, diffraction at the LHC can occur on both  $p$  sides. In the same way as we defined the kinematical variables  $x_P$  and  $\beta$  at HERA, we define  $\xi_{1,2}$  ( $= x_P$  at HERA) as the proton fractional momentum loss (or as the  $p$  momentum fraction carried by the Pomeron), and  $\beta_{1,2}$  as the fraction of the Pomeron momentum carried by the interacting parton. The produced diffractive mass is equal to  $M^2 = s\xi_1$  for single diffractive events and to  $M^2 = s\xi_1\xi_2$  for double Pomeron exchange. The size of the rapidity gap is of the order of  $\Delta\eta \sim \log 1/\xi_{1,2}$ .

The rapidity gap method can be only used at low luminosity at the LHC. At high instantaneous luminosity, many interactions (called pile-up) occur within the same bunch crossing. The pile-up interactions will fill in the rapidity gap devoid of any energy, making difficult to use the rapidity gap method. It is thus preferable to tag directly the protons at the LHC.

### 2.2. Diffraction at the LHC

In this short report, we discuss some potential measurements that can be accomplished in forward physics at the LHC. We distinguish between the low luminosity (no pile-up), medium luminosity (moderate pile-up) and high luminosity (high pile-up) environments. Forward physics is fundamental at the LHC since it addresses the QCD dynamics at the interface between hard and soft physics. For instance, the soft total  $pp$  cross section probes long transverse distances, and the BFKL [4] Pomeron is valid at short distances. In addition, diffraction and especially photon exchange processes allow performing searches beyond the Standard Model. Diffractive events are also important to tune MC and understand underlying events and soft QCD. More details about the different measurements can be found in [5].

### 2.3. LHC running conditions and forward detectors

#### 2.3.1. Forward detectors

At the LHC, the different detectors are sensitive to different programs of forward physics. The LHCf detector [6] measures the multiplicities and energy flow in the very forward direction at very low luminosity. The selection of diffractive events in LHCb [7] and ALICE [8] is performed by using the so-called rapidity gap method and will benefit from new scintillators that cover the forward region as was installed previously in CMS. The present coverage of the CMS and ATLAS forward detectors is complemented by the AFP and CMS-TOTEM/CT-PPS projects to add additional proton detectors at about 220 meters from the interaction point [9, 10].

Running at low and high  $\beta^*$  using the CMS-TOTEM, CT-PPS and ATLAS-AFP detectors allows accessing different kinematical domains for diffraction. In Fig. 5, there are displayed the acceptances in proton relative energy loss  $\xi$  versus the proton transverse momentum  $p_T$  for two values of  $\beta^*$  (0.55 m, the nominal collision optics, and 90 m) for vertical (ALFA) or horizontal (AFP) Roman Pot detector configurations located about 220 m from the ATLAS interaction point [5]. We notice that one can access low and high mass diffraction (low and high  $\xi$ ) at high  $\beta^*$  in ALFA and only low mass diffraction (up to  $\xi \sim 0.15$ ) at low  $\beta^*$  using AFP. Both measurements will be thus interesting in order to cover easily low and high mass diffraction. The kinematical coverage is similar for the vertical (CMS-TOTEM) and the horizontal pots (CT-PPS) of CMS and TOTEM.

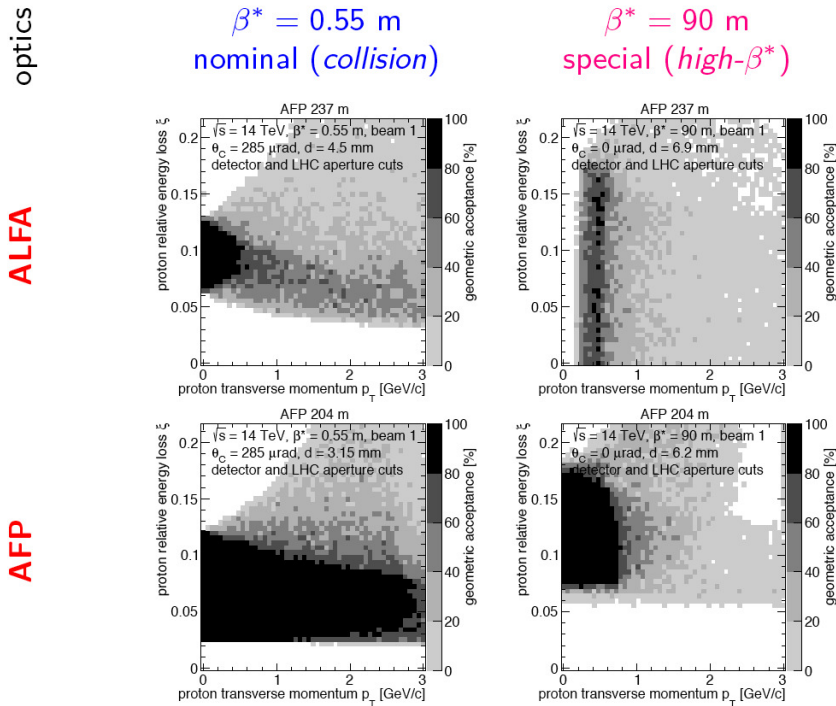


Fig. 5. Acceptance  $\xi$  versus  $t$  at low and high  $\beta^*$  for vertical (ALFA) and horizontal (AFP) Roman Pots at 220 m.

### 2.3.2. Different luminosity conditions

As we mentioned in the last section, we distinguish between the low, medium and high luminosity runs [11].

The low luminosity runs (without pile-up) allow performing multiplicity and energy flow measurements useful to tune MC as well as to measure the total and soft diffractive cross sections in the ATLAS/ALFA and TOTEM experiments. Additional measurements such as single diffraction, low mass resonances and glueballs typically require a few days of data taking (0.1 to 1. pb<sup>-1</sup>).

Medium luminosity runs are specific for the different LHC experiments. LHCb accumulate typically a few fb<sup>-1</sup> at low pile-up during their nominal data taking, while the CMS-TOTEM and ATLAS (ALFA and AFP) can accumulate low pile-up data in low and high  $\beta^*$  special runs at low luminosity at the LHC. It is then typically possible to accumulate 1 to 10 pb<sup>-1</sup> at high  $\beta^*$  with a pile-up  $\mu \sim 1$  with a few days of data taking and 10 to 100 pb<sup>-1</sup> at low  $\beta^*$  with one to two weeks of data taking at  $\mu \sim 2$  to 5.

High pile-up data taking means taking all the luminosity delivered typically to ATLAS and CMS with a pile-up  $\mu$  between 20 and 100. It is also possible to collect data at a lower pile-up  $\mu \sim 25$  by restricting to the end of store data taking (up to 40% of the total luminosity can be collected in this way) or to data originating from the tails of the vertex distribution.

### 2.4. Low luminosity measurements

In addition to measurements of the total and soft diffraction cross sections performed at high  $\beta^*$  in dedicated runs, data taken without pile-up are specially interesting to measure multiplicities and energy flow especially useful to tune MC benefiting from the different coverage in rapidity of the different LHC experiments. There is also a special interest driven by the cosmic ray community to measure the multiplicities in proton–oxygen runs at the LHC since models make different predictions in those conditions even if they lead to similar predictions in proton–proton interactions at 14 TeV. This will allow making precise predictions on proton–oxygen events for cosmic ray physics.

Another example of fundamental measurements to be performed at very low luminosity is the measurement of the size of the forward gap in diffractive events when the protons are tagged in AFP or in TOTEM. The differences between the models are much larger when the protons are tagged [5], and this will allow further tuning of the models as shown in Fig. 6.

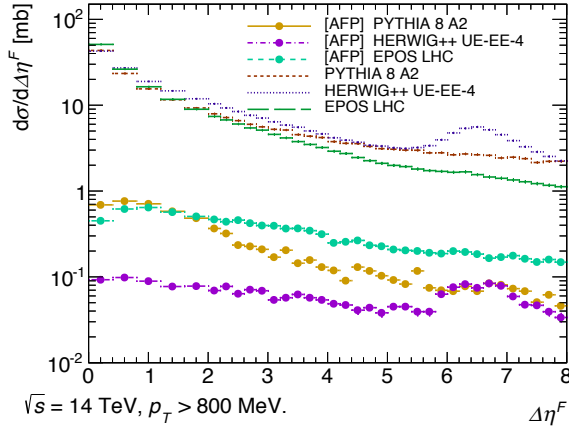


Fig. 6. Size of rapidity in diffractive events for different MC models when protons are tagged in AFP or not.

## 2.5. Medium luminosity measurements

### 2.5.1. Inclusive diffractive measurements

Medium luminosity measurements with the rapidity gap method used in ALICE (two new scintillator hodoscopes covering  $-7.0 < \eta < -4.9$  and  $4.8 < \eta < 6.3$  are being installed in ALICE in order to improve the forward coverage) or with proton tagging in AFP and CMS-TOTEM allow constraining further the Pomeron structure using  $\gamma$ +jet and di-jet events [12]. The aim is to answer mainly the following questions that are fundamental from the QCD point of view:

- Is it the same object (the same Pomeron) which explains diffraction in  $pp$  (LHC) and  $ep$  (HERA)? Are the measurements compatible between the different accelerators?
- If yes, what are the further constraints of the Pomeron structure in terms of quarks and gluons?
- What is the value of the survival probability? It is important to measure it since it is difficult to compute it theoretically, being sensitive to non-perturbative physics.

Feasibility studies have been performed in ATLAS (and measurements started in CMS-TOTEM at 8 TeV) concerning the possibility to measure jet production cross sections in single diffractive and double Pomeron exchange events at low  $\beta^*$  [5].

**2.5.2. Di-jet production in double Pomeron exchange processes and sensitivity to the gluon density in the Pomeron**

One can first probe if the Pomeron is universal between  $ep$  and  $pp$  colliders, or in other words, if we are sensitive to the same object at HERA and the LHC using as an example di-jet production in single diffractive and double Pomeron exchange at the LHC. It is possible to assess the gluon and quark densities using the di-jet and  $\gamma$ +jet productions. The different diagrams of the processes that can be studied at the LHC are shown in Fig. 7, namely double Pomeron exchange (DPE) production of di-jets (left), of  $\gamma$ +jet (middle), sensitive respectively to the gluon and quark contents of the Pomeron, and the jet-gap-jet events (right).

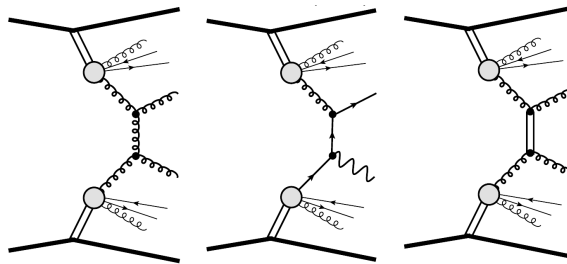


Fig. 7. Inclusive diffractive diagrams. From left to right: jet production in inclusive double Pomeron exchange,  $\gamma$ +jet production in DPE, jet-gap-jet events.

The di-jet production in DPE events at the LHC is sensitive to the gluon density in the Pomeron. In order to quantify how well we are sensitive to the Pomeron structure in terms of gluon density at the LHC, we display in Fig. 8, the di-jet mass fraction, the ratio of the di-jet mass to the total diffractive mass [12–14]. The central black line displays the cross section value for the gluon density in the Pomeron measured at HERA including an additional survival probability of 0.03. The grey/yellow band shows the effect of the 20% uncertainty on the gluon density taking into account the normalisation uncertainties. The dashed curves display how the di-jet cross section at the LHC is sensitive to the gluon density distribution especially at high  $\beta$ . For this sake, we multiply the gluon density in the Pomeron from HERA by  $(1 - \beta)^\nu$ , where  $\nu$  varies between  $-1$  and  $1$ . When  $\nu$  is equal to  $-1$  (resp.  $1$ ), the gluon density is enhanced (resp. decreased) at high  $\beta$ . We note that the curves corresponding to the different values of  $\nu$  are much more separated at high values of the di-jet mass fraction, meaning that this observable is indeed sensitive to the gluon density at high  $\beta$ .

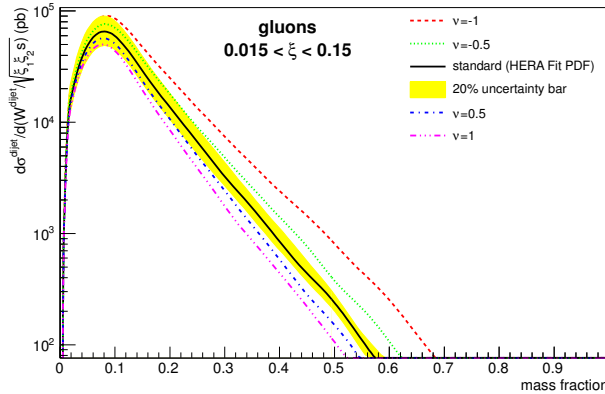


Fig. 8. DPE di-jet mass fraction distribution. The different curves correspond to different modifications of the Pomeron gluon density extracted from HERA data (see the text).

### 2.5.3. Sensitivity to the Pomeron structure in quarks using $\gamma$ +jet events and $W$ asymmetry

The QCD diffractive fits performed at HERA assumed that  $u = d = s = \bar{u} = \bar{d} = \bar{s}$ , since data were not sensitive to the difference between the different quark component in the Pomeron. On the contrary, measuring the  $\gamma$ +jet to the di-jet cross section ratios as a function of the diffractive mass  $M$  allows to distinguish between different assumptions on the quark content of the Pomeron [12]. For instance, varying  $d/u$  between 0.25 and 4 leads to a variation of the cross-section ratio by a factor 2.5. These measurements can be performed both at low and high  $\beta^*$  leading to different kinematical domains in jet and photon  $p_T$ .

In addition, it is possible to use the  $W$  asymmetry in single diffractive  $W$  production [15]. Typically, the muon asymmetry is directly sensitive to the quark content of the Pomeron and varies by a factor 6 at low  $\xi$  between the assumptions  $u/d = 2$  or  $u/d = 1/2$  for the quark content in the Pomeron.

### 2.6. Probing BFKL dynamics in diffractive events

In this subsection, we will discuss how one can probe NLL BFKL resummation effects using the gap between jets events at the LHC in double Pomeron exchanges (we will assume that the proton can be tagged in AFP or CMS/TOTEM).

The production cross section of two jets with a gap in rapidity between them reads

$$\frac{d\sigma^{pp \rightarrow XJJY}}{dx_1 dx_2 dE_T^2} = \mathcal{S} f_{\text{eff}}(x_1, E_T^2) f_{\text{eff}}(x_2, E_T^2) \frac{d\sigma^{gg \rightarrow gg}}{dE_T^2}, \quad (3)$$

where  $\sqrt{s}$  is the total energy of the collision,  $E_T$  the transverse momentum of the two jets,  $x_1$  and  $x_2$  their longitudinal fraction of momentum with respect to the incident hadrons,  $\mathcal{S}$  the survival probability, and  $f$  the effective parton density functions [16]. The rapidity gap between the two jets is  $\Delta\eta = \ln(x_1 x_2 s / p_T^2)$ .

The cross section is given by

$$\frac{d\sigma^{gg \rightarrow gg}}{dE_T^2} = \frac{1}{16\pi} |A(\Delta\eta, E_T^2)|^2 \quad (4)$$

in terms of the  $gg \rightarrow gg$  scattering amplitude  $A(\Delta\eta, p_T^2)$ .

In the following, we consider the high energy limit in which the rapidity gap  $\Delta\eta$  is assumed to be very large. The BFKL framework allows to compute the  $gg \rightarrow gg$  amplitude in this regime, and the result is known up to NLL accuracy

$$A(\Delta\eta, E_T^2) = \frac{16N_c\pi\alpha_s^2}{C_F E_T^2} \sum_{p=-\infty}^{\infty} \int \frac{d\gamma}{2i\pi} A_p, \quad (5)$$

$$A_p = \frac{[p^2 - (\gamma - 1/2)^2] \exp\{\bar{\alpha}(E_T^2) \chi_{\text{eff}}[2p, \gamma, \bar{\alpha}(E_T^2)] \Delta\eta\}}{[(\gamma - 1/2)^2 - (p - 1/2)^2][(\gamma - 1/2)^2 - (p + 1/2)^2]} \quad (6)$$

with the complex integral running along the imaginary axis from  $1/2 - i\infty$  to  $1/2 + i\infty$ , and with only even conformal spins contributing to the sum, and  $\bar{\alpha} = \alpha_s N_c / \pi$  the running coupling.

In this study, we performed a parametrised distribution of  $d\sigma^{gg \rightarrow gg} / dE_T^2$  so that it can be easily implemented in the HERWIG Monte Carlo [17] since performing the integral over  $\gamma$  in particular would be too much time consuming in a Monte Carlo. The implementation of the BFKL cross section in a Monte Carlo is absolutely necessary to make a direct comparison with data. Namely, the measurements are sensitive to the jet size (for instance, experimentally, the gap size is different from the rapidity interval between the jets which is not the case by definition in the analytic calculation).

It is thus possible to detect jet-gap-jet events in diffractive double Pomeron exchange processes [16]. The idea is to tag the intact protons inside the AFP and CMS/TOTEM forward proton detectors [10] located at about 220 m from the ATLAS and CMS interaction points on both sides.

The advantage of such processes is that they are quite clean since they are not “polluted” by proton remnants and it is possible to go to larger jet separation than for usual jet–gap–jet events. The normalisation for these processes come from the fit to the D0 jet–gap–jet measurements discussed in Ref. [16]. The ratio between jet–gap–jet to inclusive jet events is shown in Fig. 9 requesting protons to be tagged in AFP for both samples. The ratio shows a weak dependence as a function of jet  $p_T$  (and also as a function of the difference in rapidity between the two jets). It is worth noticing that the ratio is about 20–30% showing that the jet–gap–jet events are much more present in the diffractive sample than in the inclusive one as expected.

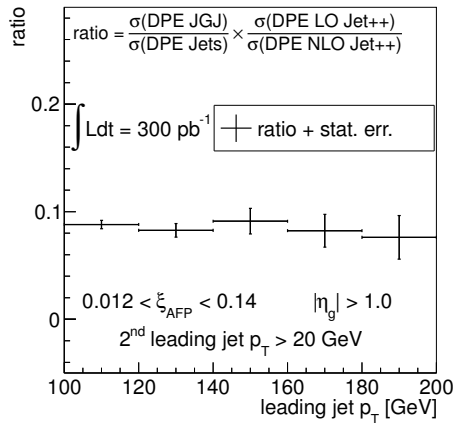


Fig. 9. Ratio of the jet–gap–jet to the inclusive jet cross sections at the LHC as a function of jet  $p_T$  in double Pomeron exchange events where the protons are detected in AFP or TOTEM.

### 2.7. Exclusive diffraction

The advantage of the exclusive diffractive and photon exchange processes illustrated in Fig. 10 is that all particles can be measured in the final state. Both protons can be measured in AFP or CMS-TOTEM and the produced particles (jets, vector mesons,  $Z$  boson ...) in ATLAS or CMS, and there is no energy losses such as in the Pomeron remnants as shown in Fig. 10, left diagram. It is thus possible to reconstruct the properties of the object produced exclusively (via photon and gluon exchanges) from the tagged proton since the system is completely constrained. It is worth mentioning that it is also possible to constrain the background by asking the matching between the information of the two protons and the produced object, and

thus, central exclusive production is a potential channel for beyond Standard Model physics at high masses [9] in the ATLAS and CMS collaborations as we will see in the following.

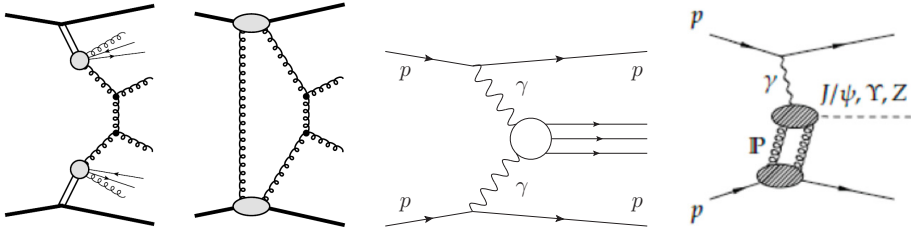


Fig. 10. Exclusive diffractive and photon exchange processes. The left diagram shows the double Pomeron exchange event for reference, the second one — the QCD exclusive production, the third one — the production of a system  $X$  via photon exchanges, and the last one — the exclusive photo-production events.

Exclusive vector mesons can be also measured in the LHCb experiment which recently, for the first time, measured the diffractive production of charmonium [18]. The Herschel scintillators are now being installed in LHCb to enhance the coverage at high rapidities in order to get a better control of non-exclusive background. Such channels are also sensitive to new physics: if a medium mass resonance due to a glueball or a tetraquark state exists, it could lead to a bump in the invariant mass distribution of the charmonium states.

The CMS/TOTEM experiment also performed extensive studies of possible measurements of exclusive states at high  $\beta^*$ . It is worth mentioning that the search for glueball states and the probe of the low  $x$  gluon density down to  $x \sim 10^{-4}$  will be possible. With  $1 \text{ pb}^{-1}$ , it will be possible to confirm or not the existence of the unobserved possible  $f_0(1710)$  and  $f_0(1500)$  decay modes and with 5 to  $10 \text{ pb}^{-1}$ , the unambiguous spin determination and the precise measurement of cross section times branching ratio. In addition, the measurement of the cross section times branching ratio for the three  $\chi_{C,0,1,2}$  states, will be performed allowing a comparison with the results to the LHCb measurement [19] and the exclusive QCD calculations [20].

In addition, it is possible to measure the exclusive di-jet production at the LHC with about  $40 \text{ fb}^{-1}$  and a pile-up of 40 as was shown by the ATLAS and CT-PPS collaborations. Despite the high level of pile-up background, it is possible to obtain a pure enough of exclusive jets that can further constrain the models of exclusive diffractive production [10].

### 3. Photon induced processes at the LHC and anomalous coupling studies

In this section, we discuss some potential measurements to be performed using proton tagging detectors at the LHC based on  $\gamma$ -induced processes. The main motivation is to explore rare events, searching for beyond Standard Model physics such as quartic anomalous couplings between photons and  $W/Z$  bosons and photons. We assume, as usual, in the following intact protons to be tagged in CMS/TOTEM or in AFP. These studies regained recently high interest with the observation of a potential resonance decaying into  $\gamma\gamma$  at about 750 GeV that was observed by the ATLAS and CMS collaborations as we will see in the following [21, 22].

In the first part of this section, we discuss the SM production of  $W$  and  $\gamma$  pairs at the LHC via photon exchanges. In the second, third and fourth subsections, we discuss the sensitivities of these processes to trilinear and quartic gauge anomalous couplings, and we finish by discussing the role of photon-induced processes in the existence of a potential new resonance decaying into two photons.

#### 3.1. Standard Model exclusive $\gamma\gamma$ , $WW$ and $ZZ$ production

In Fig. 11, we show the leading processes leading to two photons and two intact protons in the final state as an example. The first diagram (left) corresponds to exclusive QCD di-photon production via gluon exchanges (the second gluon ensures that the exchange is colourless leading to intact protons in the final state) and the second one (right) via photon exchanges. It is worth noticing that quark, lepton and  $W$  loops need to be considered in order to get the correct SM cross section for di-photon production as shown in Fig. 12. The QCD-induced processes from the Khoze–Martin–Ryskin model [20] are dominant at low masses, whereas the photon-induced ones (QED processes) dominate at higher di-photon masses [23]. It is very

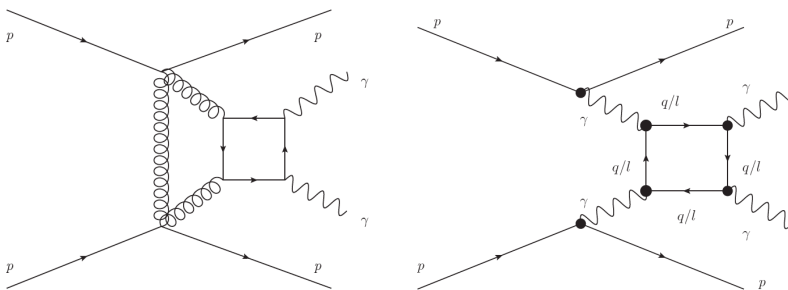


Fig. 11. Left: Di-photon QCD exclusive production. Right: Di-photon production via photon exchanges.

important to notice that the  $W$  loop contribution dominates at high di-photon masses [23] whereas this contribution is omitted in most studies. This is the first time that we put all terms inside a MC generator, FPMC [24].

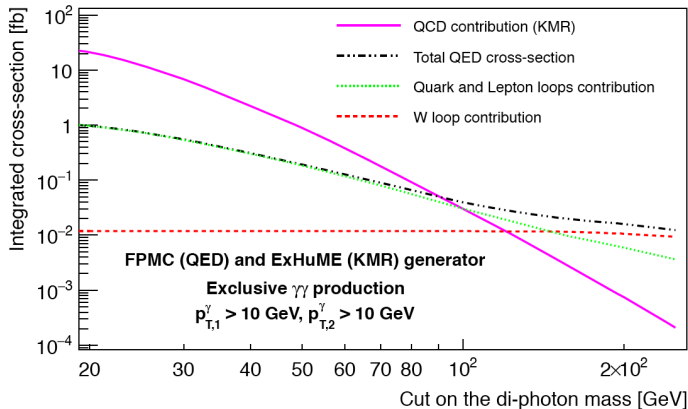


Fig. 12. Di-photon production cross section as a function of the di-photon mass requesting two intact protons in the final state and the photons to have a transverse momentum larger than 10 GeV. The QCD exclusive processes (Khoze–Martin–Ryskin) in full line dominate at low masses, while QED di-photon production dominates at higher masses (dashed lines). The QED production corresponds to di-photon production via lepton/fermion loops (dotted line) and  $W$  boson loops (dash-dotted line).

The Standard Model of  $W$  pair production via gluon or photon-induced processes was also implemented in FPMC leading to a cross section of about 96 fb at a center-of-mass energy of 14 TeV, and it is clear that the exclusive production of  $Z$  boson pairs is forbidden in the Standard Model.

### 3.2. Triple anomalous gauge couplings

In Ref. [25], we also studied the sensitivity to triple gauge anomalous couplings at the LHC. The Lagrangian including anomalous triple gauge couplings  $\lambda^\gamma$  and  $\Delta\kappa^\gamma$  is the following

$$\mathcal{L} \sim \left( W_{\mu\nu}^\dagger W^\mu A^\nu - W_{\mu\nu} W^{\dagger\mu} A^\nu \right) + (1 + \Delta\kappa^\gamma) W_\mu^\dagger W_\nu A^{\mu\nu} + \frac{\lambda^\gamma}{M_W^2} W_{\rho\mu}^\dagger W^\mu{}_\nu A^{\nu\rho}. \quad (7)$$

The strategy was the following: we first implemented this Lagrangian in FPMC [24] and we selected the signal events when the  $Z$  and  $W$  bosons decay into leptons so that the background would be negligible (the decays into jets

would be more complicated because of the high QCD di-jet background). The difference is that the signal appears at high mass for  $\lambda^\gamma$  and  $\Delta\kappa^\gamma$  only modifies the normalization and the low mass events have to be retained. The sensitivity on triple gauge anomalous couplings is a gain of about a factor 3 with respect to the LEP limits, which represents one of the best reaches at the LHC.

### 3.3. Quartic $WW$ and $ZZ$ anomalous couplings

In this section, we will study the reach at the LHC concerning the  $\gamma\gamma WW$  and  $\gamma\gamma ZZ$  anomalous coupling. The principle is always similar: we select photon-induced processes leading to two intact protons and either  $W$  or  $Z$  pairs in the final state. The protons are measured in CMS/TOTEM or AFP and the  $W$ s and  $Z$ s in CMS and ATLAS.

The parameterization of the quartic couplings based on [26] is adopted. The cuts to select quartic anomalous gauge coupling  $WW$  events are the following, namely  $0.015 < \xi < 0.15$  for the tagged protons corresponding to the AFP or CT-PPS detector at 210 and 420 m,  $\cancel{E}_T > 20$  GeV,  $\Delta\phi < 3.13$  between the two leptons. In addition, a cut on the  $p_T$  of the leading lepton  $p_T > 160$  GeV and on the diffractive mass  $W > 800$  GeV are requested since anomalous coupling events appear at high mass. After these requirements, we expect about 0.7 background events for an expected signal of 17 events if the anomalous coupling is about four orders of magnitude lower than the present LEP limit [27] ( $|a_0^W/\Lambda^2| = 5.4 \cdot 10^{-6}$ ) or two orders of magnitude lower with respect to the D0 and CMS limits [28] for a luminosity of  $30 \text{ fb}^{-1}$ . The strategy to select anomalous coupling  $ZZ$  events is analogous and the presence of three leptons or two-like sign leptons are requested. Table I gives the reach on anomalous couplings at the LHC for luminosities of 30 and  $200 \text{ fb}^{-1}$  compared to the present OPAL limits from the LEP accelerator [27].

Figure 13 shows respectively the number of expected events for signal as a function of the anomalous coupling value and the  $5\sigma$  discovery contours for all  $WW$  and  $ZZ$  anomalous couplings for 30 and  $200 \text{ fb}^{-1}$ . It is possible to reach the values expected in extra dimension models. The tagging of the protons using the ATLAS and CMS Forward Physics detectors is likely to be the only method to probe such small values of quartic anomalous couplings.

The search for quartic anomalous couplings between  $\gamma$  and  $W$  bosons was performed again after a full simulation of the ATLAS and CMS detectors including pile up [10] assuming the protons to be tagged in AFP or CT-PPS at 210 m only. Integrated luminosities of 40 and  $300 \text{ fb}^{-1}$  with, respectively, 23 or 46 average pile-up events per beam crossing have been considered and lead to similar results. In order to reduce the background, each  $W$  is assumed to decay leptonically (note that the semi-leptonic case

in under study). The full list of background processes used for the ATLAS measurement of Standard Model  $WW$  cross section was simulated, namely  $t\bar{t}$ ,  $WW$ ,  $WZ$ ,  $ZZ$ ,  $W$ +jets, Drell–Yan and single top events.

TABLE I

Reach on anomalous couplings obtained in  $\gamma$ -induced processes after tagging the protons in AFP or CT-PPS compared to the present OPAL limits. The  $5\sigma$  discovery and 95% C.L. limits are given for a luminosity of 30 and 200  $\text{fb}^{-1}$  [25, 29].

Couplings	OPAL limits [ $\text{GeV}^{-2}$ ]	Sensitivity @ $\mathcal{L} = 30$ (200) $\text{fb}^{-1}$	
		$5\sigma$	95% C.L.
$a_0^W/\Lambda^2$	$[-0.020, 0.020]$	$5.4 \cdot 10^{-6}$ ( $2.710^{-6}$ )	$2.6 \cdot 10^{-6}$ ( $1.410^{-6}$ )
$a_C^W/\Lambda^2$	$[-0.052, 0.037]$	$2.0 \cdot 10^{-5}$ ( $9.610^{-6}$ )	$9.4 \cdot 10^{-6}$ ( $5.210^{-6}$ )
$a_0^Z/\Lambda^2$	$[-0.007, 0.023]$	$1.4 \cdot 10^{-5}$ ( $5.510^{-6}$ )	$6.4 \cdot 10^{-6}$ ( $2.510^{-6}$ )
$a_C^Z/\Lambda^2$	$[-0.029, 0.029]$	$5.2 \cdot 10^{-5}$ ( $2.010^{-5}$ )	$2.4 \cdot 10^{-5}$ ( $9.210^{-6}$ )

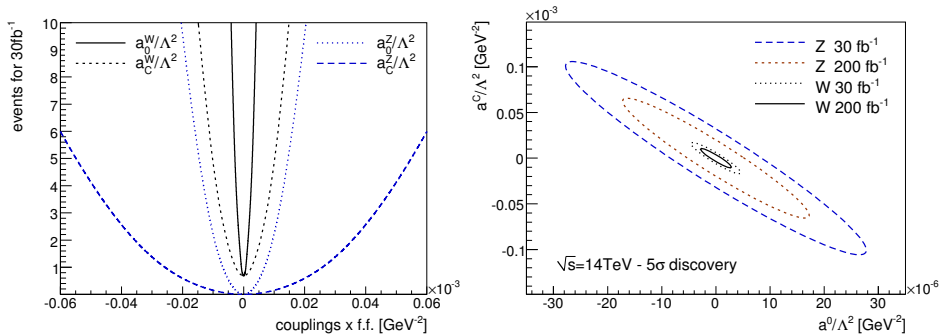


Fig. 13. Left: Number of events for signal due to different values of anomalous couplings after all cuts (see the text) for a luminosity of  $30 \text{ fb}^{-1}$ . Right:  $5\sigma$  discovery contours for all the  $WW$  and  $ZZ$  quartic couplings at  $\sqrt{s} = 14 \text{ TeV}$  for a luminosity of  $30 \text{ fb}^{-1}$  and  $200 \text{ fb}^{-1}$ .

### 3.4. Quartic photon anomalous couplings

#### 3.4.1. Theoretical motivations

In this section, four-photon ( $4\gamma$ ) interactions through di-photon production via photon fusion with intact outgoing protons are considered. We will give an historical perspective starting from a sensitivity study to anomalous

$\gamma\gamma\gamma\gamma$  that was performed before the observation of a potential resonance by the CMS and ATLAS collaborations at a di-photon mass of 750 GeV, and we will discuss the relevance of this observation with respect to this study in the following subsection.

In the assumption of a new physics mass scale  $\Lambda$  heavier than the experimentally accessible energy  $E$ , all new physics manifestations can be described using an effective Lagrangian valid for  $\Lambda \gg E$ . Among these operators, the pure photon dimension-eight operators

$$\mathcal{L}_{4\gamma} = \zeta_1^\gamma F_{\mu\nu} F^{\mu\nu} F_{\rho\sigma} F^{\rho\sigma} + \zeta_2^\gamma F_{\mu\nu} F^{\nu\rho} F_{\rho\lambda} F^{\lambda\mu} \quad (8)$$

can induce the  $\gamma\gamma\gamma\gamma$  process, highly suppressed in the SM [23, 30]. We discuss here possible new physics contributions to  $\zeta_{1,2}^\gamma$  that can be probed and discovered at the LHC using the forward proton detectors.

Loops of heavy charged particles contribute to the  $4\gamma$  couplings [23, 30] as  $\zeta_i^\gamma = \alpha_{\text{em}}^2 Q^4 m^{-4} N c_{i,s}$ , where  $c_{1,s}$  is related to the spin of the heavy particle of mass  $m$  running in the loop and  $Q$  its electric charge. The factor  $N$  counts all additional multiplicities such as colour or flavour. These couplings scale as  $\sim Q^4$  and are enhanced in presence of particles with large charges. For example, certain light composite fermions, characteristic of composite Higgs models, have typically electric charges of several units. For a 500 GeV vector (fermion) resonance with  $Q = 3$  (4), large couplings  $\zeta_i^\gamma$  of the order of  $10^{-13}$ – $10^{-14}$  GeV $^{-4}$  can be reached.

Beyond perturbative contributions to  $\zeta_i^\gamma$  from charged particles, non-renormalizable interactions of neutral particles are also present in common extensions of the SM. Such theories can contain scalar, pseudo-scalar and spin-2 resonances that couple to the photon and generate the  $4\gamma$  couplings by tree-level exchange as  $\zeta_i^\gamma = (f_s m)^{-2} d_{i,s}$ , where  $d_{1,s}$  is related to the spin of the particle. Strongly-coupled conformal extensions of the SM contain a scalar particle ( $s = 0^+$ ), the dilaton. Even a 2 TeV dilaton can produce a sizable effective photon interaction,  $\zeta_1^\gamma \sim 10^{-13}$  GeV $^{-4}$ . These features are reproduced at large number of colours by the gauge-gravity correspondence in a warped extra dimension. Warped-extra dimensions also feature Kaluza–Klein (KK) gravitons [31], that can induce anomalous couplings [30]

$$\zeta_i^\gamma = \frac{\kappa^2}{8\tilde{k}^4} d_{i,2}, \quad (9)$$

where  $\tilde{k}$  is the IR scale that determines the first KK graviton mass and  $\kappa$  is a parameter that can be taken  $\mathcal{O}(1)$ . For  $\kappa \sim 1$ , and  $m_2 \lesssim 6$  TeV, the photon vertex can easily exceed  $\zeta_2^\gamma \sim 10^{-14}$  GeV $^{-4}$ .

### 3.4.2. Experimental sensitivity to quartic four photon couplings

The  $\gamma\gamma\gamma\gamma$  process (Fig. 11 (left)) can be probed via the detection of two intact protons in the forward proton detectors and two energetic photons in the corresponding electromagnetic calorimeters [23]. The SM cross section of di-photon production with intact protons is dominated by the QED process at high di-photon mass — and not by gluon exchanges — and is thus very well-known, as we saw in the previous section.

As mentioned in Ref. [32], the photon identification efficiency is expected to be around 75% for  $p_T > 100$  GeV, with jet rejection factors exceeding 4000 even at high pile-up ( $> 100$ ). In addition, about 1% of the electrons are mis-identified as photons. These numbers are used in the phenomenological study presented below. For these studies, we used as an example the ATLAS inefficiencies of identifying a photon, the mis-identification probabilities of a jet or a lepton into a photon, and the resolution in energy and rapidities for photons, as well as probability for conversion in lepton pairs.

As for the previous studies, the anomalous  $\gamma\gamma\gamma\gamma$  process has been implemented in the Forward Physics Monte Carlo (FPMC) generator [24]. The FPMC generator was also used to simulate the background processes giving rise to two intact protons accompanied by two photons, electrons or jets that can mimic the photon signal. Those include exclusive SM production of  $\gamma\gamma\gamma\gamma$  via lepton and quark boxes and  $\gamma\gamma \rightarrow e^+e^-$ . The central exclusive production of  $\gamma\gamma$  via two-gluon exchange, not present in FPMC, was simulated using ExHuME [33]. This series of backgrounds is called “Exclusive” in Table II and Figs. 14, 15. FPMC was also used to produce  $\gamma\gamma$ , Higgs to  $\gamma\gamma$  and di-jet productions via double Pomeron exchange (called DPE background in Table II and Fig. 14). Such backgrounds tend to be softer than the signal and can be suppressed with requirements on the transverse momenta of the photons and the di-photon invariant mass. In addition, the final-state photons of the signal are typically back-to-back and have about the same transverse momenta. Requiring a large azimuthal angle  $|\Delta\phi| > \pi - 0.01$  between the two photons and a ratio  $p_{T,2}/p_{T,1} > 0.95$  greatly reduces the contribution of non-exclusive processes.

Additional background processes include the quark and gluon-initiated production of two photons, two jets and Drell–Yan processes leading to two electrons. The two intact protons arise from pile-up interactions (these backgrounds are called  $\gamma\gamma+$  pile-up and  $e^+e^-$ , di-jet + pile-up in Table II). These events were produced using HERWIG [17] and PYTHIA [34]. The pile-up background is further suppressed by requiring the proton missing invariant mass to match the di-photon invariant mass within the expected resolution and the di-photon system rapidity and the rapidity of the two protons to be similar (see Fig. 15).

TABLE II

Number of signal for  $Q_{\text{eff}} = 4$ ,  $m = 340$  GeV and background events after various selections for an integrated luminosity of  $300 \text{ fb}^{-1}$  and  $\mu = 50$  at  $\sqrt{s} = 14$  TeV. Values obtained using the corresponding EFT couplings with and without form factors are also displayed. Excl. stands for exclusive backgrounds and DPE for double Pomeron exchange backgrounds.

Cut/Process	Signal (full)	Signal with/without f.f. (EFT)	Excl.	DPE	DY di-jet+ pile-up	$\gamma\gamma$ + pile-up
$[0.015 < \xi_{1,2} < 0.15,$ $p_{T1,(2)} > 200$ $(100) \text{ GeV}]$	65.	18.(187.)	0.13	0.2	1.6	2968
$m_{\gamma\gamma} > 600 \text{ GeV}$	64.	17.(186.)	0.10	0	0.2	1023
$p_{T2}/p_{T1} > 0.95,$ $ \Delta\phi  > \pi - 0.01$	64.	17.(186.)	0.10	0	0	80.2
$\sqrt{\xi_1 \xi_2 s} = m_{\gamma\gamma} \pm 3\%$	61.	12.(175.)	0.09	0	0	2.8
$ y_{\gamma\gamma} - y_{pp}  < 0.03$	60.	16.(169.)	0.09	0	0	0

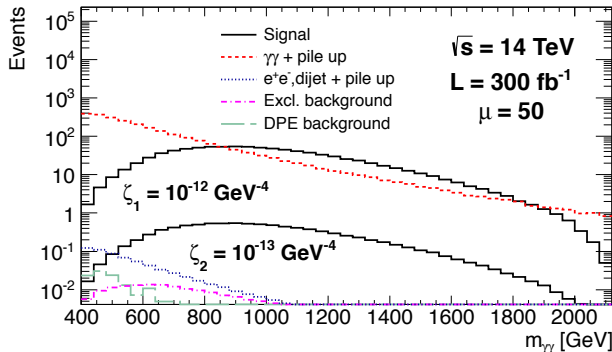


Fig. 14. Di-photon invariant mass distribution for the signal ( $\zeta_1 = 10^{-12}$ ,  $10^{-13} \text{ GeV}^{-4}$ , see Eq. (8)) and for the backgrounds (dominated by  $\gamma\gamma$  with protons from pile-up), requesting two protons in the forward detectors and two photons of  $p_T > 50$  GeV with at least one converted photon in the central detector, for a luminosity of  $300 \text{ fb}^{-1}$  and an average pile-up of  $\mu = 50$ .

The number of expected signal and background events passing respective selections is shown in Table II for an integrated luminosity of  $300 \text{ fb}^{-1}$  for a center-of-mass energy of 14 TeV [23]. Exploiting the full event kinematics with the forward proton detectors allows to completely suppress the background with a signal selection efficiency after the acceptance cuts exceeding

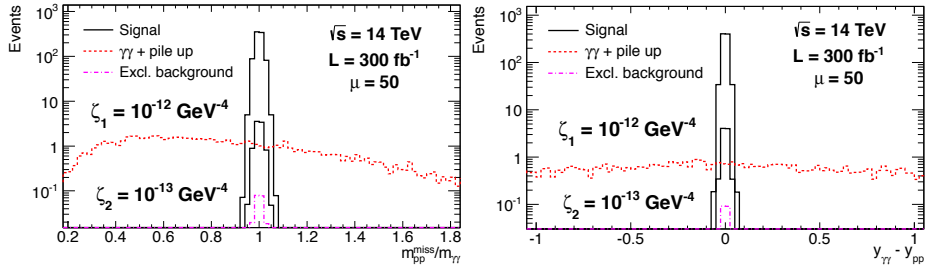


Fig. 15. Diphoton to missing proton mass ratio (left) and rapidity difference (right) distributions for signal considering two different coupling values ( $10^{-12}$  and  $10^{-13}$   $\text{GeV}^{-4}$ , see Eq. (8)) and for backgrounds after requirements on photon  $p_T$ , di-photon invariant mass,  $p_T$  ratio between the two photons and on the angle between the two photons. At least one converted photon is required. The integrated luminosity is  $300 \text{ fb}^{-1}$  and the average pile-up is  $\mu = 50$ .

70%. Tagging the protons is absolutely needed to suppress the  $\gamma\gamma$  + pile-up events. Further background reduction is even possible by requiring the photons and the protons to originate from the same vertex that provides an additional rejection factor of 40 for 50 pile-up interactions, showing the large margin on the background suppression. A similar study at a higher pile-up of 200 was performed and led to a very small background. The sensitivities on photon quartic anomalous couplings are given in Table III. The sensitivity extends up to  $7 \times 10^{-15}$   $\text{GeV}^{-4}$  allowing us to probe further the models of new physics described above.

TABLE III

$5\sigma$  discovery and 95% C.L. exclusion limits on  $\zeta_1$  and  $\zeta_2$  couplings in  $\text{GeV}^{-4}$  (see Eq. (8)) with and without form factor (f.f.), requesting at least one converted photon ( $\geq 1$  conv.  $\gamma$ ) or not (all  $\gamma$ ). All sensitivities are given for  $300 \text{ fb}^{-1}$  and  $\mu = 50$  pile-up events (medium luminosity LHC) except for the numbers of the last column which are given for  $3000 \text{ fb}^{-1}$  and  $\mu = 200$  pile-up events (high luminosity LHC).

Luminosity pile-up ( $\mu$ )	$300 \text{ fb}^{-1}$ 50	$300 \text{ fb}^{-1}$ 50	$300 \text{ fb}^{-1}$ 50	$300 \text{ fb}^{-1}$ 50	$3000 \text{ fb}^{-1}$ 200
Coupling [ $\text{GeV}^{-4}$ ]	$\geq 1$ conv. $\gamma$ $5\sigma$	$\geq 1$ conv. $\gamma$ 95% C.L.	all $\gamma$ $5\sigma$	all $\gamma$ 95% C.L.	all $\gamma$ 95% C.L.
$\zeta_1$ f.f.	$8 \times 10^{-14}$	$5 \times 10^{-14}$	$4.5 \times 10^{-14}$	$3 \times 10^{-14}$	$2.5 \times 10^{-14}$
$\zeta_1$ no f.f.	$2.5 \times 10^{-14}$	$1.5 \times 10^{-14}$	$1.5 \times 10^{-14}$	$9 \times 10^{-15}$	$7 \times 10^{-15}$
$\zeta_2$ f.f.	$2 \times 10^{-13}$	$1 \times 10^{-13}$	$9 \times 10^{-14}$	$6 \times 10^{-14}$	$4.5 \times 10^{-14}$
$\zeta_2$ no f.f.	$5 \times 10^{-14}$	$4 \times 10^{-14}$	$3 \times 10^{-14}$	$2 \times 10^{-14}$	$1.5 \times 10^{-14}$

We also performed a full amplitude calculation in Ref. [23] that avoids the dependence on the choice of form factors needed in order to avoid quadratic divergences of scattering amplitudes. Sensitivities were found to be similar leading to possible discoveries of vector or fermions at high masses and high effective charges.

If discovered at the LHC,  $\gamma\gamma\gamma\gamma$  quartic anomalous couplings would be a major discovery related to the existence of extra dimensions in the universe as an example. In addition, it might be investigated if there could be a link with some experiments in atomic physics, for instance, the intrication experiments that might be interpreted via the existence of extra dimensions. Furthermore, it is clear that extra dimensions might be relevant also for the fast expansion of the universe within inflation models.

*3.5. Photon quartic anomalous couplings and the potential presence of a resonance in the di-photon mass spectrum at 750 GeV observed by the ATLAS and CMS collaborations*

Recently, the CMS and ATLAS collaborations announced the presence of a small excess in the di-photon mass spectrum for a mass of about 750 GeV at a center-of-mass energy of 13 TeV. While it is still too early to know if this excess is real or a statistical fluctuation, it is important to know how proton forward detectors might be able to give information about the production mechanism. Two experimental facts were observed: the excess is not present or is very small at a center-of-mass energy of 8 TeV, and not seen in the di-jet channel at 13 TeV. If processes were gluon-induced, we would expect the di-jet cross section to be of the order of 1 pb since the ratio of the di-jet to di-photon cross section is of the order of  $\Gamma_{gg}/\Gamma_{\gamma\gamma} = \alpha_S^2/\alpha^2 \sim 200$ . Since no excess is observed in the di-jet channel, it seems natural to consider photon-induced processes (it is clear that the potential resonance might also be produced in a combination of photon and gluon-induced processes).

In Section 3.1, we already showed that the di-photon production via photon exchanges completely dominates the one via gluon exchanges at high di-photon masses. This means that we are sure that di-photon production is photon-induced as we tag the intact protons in the final state for a di-photon resonance of about 750 GeV.

Concerning the excess that has been presently observed, the forward protons detectors were not included in data taking. This means that, for most of the events, protons were destroyed in the final state corresponding to inelastic events. The cross section of the  $pp \rightarrow R \rightarrow \gamma\gamma X$  reads [22]

$$\sigma_{pp \rightarrow \gamma\gamma X} = (7.3 \text{ fb}) \left( \frac{5 \text{ TeV}}{f_\gamma} \right)^4 \left( \frac{45 \text{ GeV}}{\Gamma_{\text{tot}}} \right) \left( \frac{r_{\text{inel}}}{20} \right), \quad (10)$$

where  $f_\gamma$ ,  $\Gamma_{\text{tot}}$ ,  $r_{\text{inel}}$  are, respectively, the  $\gamma\gamma R$  coupling, the width of the resonance, and the ratio between the inelastic and elastic contributions. As determined by data,  $f_\gamma$  is of the order of 5 TeV, and the width  $\Gamma_{\text{tot}}$  of the order of 45 GeV. The  $r_{\text{inel}}$  parameter is about 20 with a large uncertainty. More recent studies lead to a better determination of this factor [35]. The fact that the resonance can be produced at 13 TeV but almost not at 8 TeV is related to the probability to emit quasi-real photons from the proton that can couple to the resonance  $R$ . The phase space producing a 750 GeV resonance at a center-of-mass energy of 8 TeV is much reduced compared to 13 TeV. We estimated this factor to be between 2.4 and 3.9.

Observing di-photon exclusive production and tagging the intact protons in the final state will allow for being certain that these processes are photon-induced. As we mentioned already, this is a background-free experiment, which means that the observation of 5 events is enough to obtain a  $5\sigma$  discovery. We predict the following cross section for the  $pp \rightarrow p\gamma\gamma p$  process

$$\sigma_{pp \rightarrow \gamma\gamma pp} = (0.23 \text{ fb}) \left( \frac{5 \text{ TeV}}{f_\gamma} \right)^4 \left( \frac{45 \text{ GeV}}{\Gamma_{\text{tot}}} \right) r_{fs}, \quad (11)$$

where  $r_{fs}$  is the survival probability that can be estimated to be of the order of 0.8. About  $20 \text{ fb}^{-1}$  is thus necessary to obtain a  $5\sigma$  discovery in this channel.

In addition to the  $\gamma\gamma$  channel, we predict a possible significant production of  $ZZ$ ,  $WW$ , and  $Z\gamma$  events and it would be also interesting to look in these channels with tagged protons as well.

#### 4. Conclusion

In this report, we detailed the interest of tagging the intact protons to study in detail the Pomeron structure in terms of quarks and gluons and  $WW$ ,  $ZZ$  and  $\gamma\gamma$  productions via photon exchanges. Unprecedented sensitivities can be achieved at the LHC in the CMS-TOTEM and ATLAS experiments on quartic anomalous couplings, especially on  $\gamma\gamma\gamma\gamma$  couplings, that will lead to one of the best sensitivity on extra dimensions at the LHC, and to potential discoveries if the existence of the di-photon resonance is confirmed.

#### REFERENCES

- [1] H. Navelet, R. Peschanski, C. Royon, *Phys. Lett. B* **366**, 329 (1996);  
 H. Navelet, R. Peschanski, C. Royon, S. Wallon, *Phys. Lett. B* **385**, 357 (1996);  
 A. Bialas, R. Peschanski, C. Royon, *Phys. Rev. D* **57**, 6899 (1998).

- [2] G. Altarelli, G. Parisi, *Nucl. Phys. B* **126**, 298 (1977); V.N. Gribov, L.N. Lipatov, *Sov. J. Nucl. Phys.* **15**, 438 (1972); **15**, 675 (1972); Yu.L. Dokshitzer, *Sov. Phys. JETP*. **46**, 641 (1977).
- [3] H1 Collaboration, *Eur. Phys. J. C* **48**, 715 (2006) [arXiv:hep-ex/0606004]; *Eur. Phys. J. C* **48**, 749 (2006) [arXiv:hep-ex/0606003]; ZEUS Collaboration, *Nucl. Phys. B* **713**, 3 (2005); C. Royon *et al.*, *Phys. Rev. D* **63**, 074004 (2001); *Nucl. Phys. B* **781**, 1 (2007).
- [4] V.S. Fadin, E.A. Kuraev, L.N. Lipatov, *Phys. Lett. B* **60**, 50 (1975); I.I. Balitsky, L.N. Lipatov, *Sov. J. Nucl. Phys.* **28**, 822 (1978).
- [5] Report from the LHC Forward Physics Working Group, N. Cartiglia, C. Royon (Eds.), to be published in *J. Phys. G*.
- [6] LHCf Collaboration, for results see: [hep.fi.infn.it/LHCf/](http://hep.fi.infn.it/LHCf/)
- [7] LHCb Collaboration, for results see: <http://lhcb.web.cern.ch/lhcb/Physics-Results/LHCb-Physics-Results>
- [8] ALICE Collaboration, for results see: <https://twiki.cern.ch/twiki/bin/view/ALICEpublic/ALICEPublicResults>
- [9] A special issue on Central Exclusive Production in Hadron–Hadron Collisions, *Int. J. Mod. Phys. A* **29**, number 28 (2014), Eds.: M. Albrow, V. Khoze, C. Royon.
- [10] ATLAS Collaboration, CERN-LHCC-2011-012; TOTEM Collaboration, CERN-LHCC-2014-020; CMS and TOTEM collaborations, CERN-LHCC-2014-021.
- [11] A special issue on Diffractive Processes in Lepton–Hadron and Hadron–Hadron Collisions, *Int. J. Mod. Phys. A* **30**, number 08 (2015), Ed. C. Royon.
- [12] C. Marquet, C. Royon, M. Saimpert, D. Werder, *Phys. Rev. D* **88**, 074029 (2013).
- [13] C. Royon, M. Saimpert, O. Kepka, R. Zlebcik, *Acta Phys. Pol. B Proc. Suppl.* **7**, 735 (2014).
- [14] O. Kepka, C. Royon, *Phys. Rev. D* **76**, 034012 (2007).
- [15] A. Chuinard, C. Royon, R. Staszewski, *J. High Energy Phys.* **1604**, 092 (2016).
- [16] C. Marquet, C. Royon, M. Trzebinski, R. Zlebcik, *Phys. Rev. D* **87**, 034010 (2013); O. Kepka, C. Marquet, C. Royon, *Phys. Rev. D* **83**, 034036 (2011).
- [17] G. Corcella *et al.*, arXiv:hep-ph/0210213.
- [18] LHCb Collaboration, *J. Phys. G* **41**, 115002 (2014) [arXiv:1407.5973 [hep-ex]].
- [19] LHCb Collaboration, see: <https://twiki.cern.ch/twiki/bin/view/LHCb/PrelimExclDiMu>
- [20] V.A. Khoze, A.D. Martin, M.G. Ryskin, *Eur. Phys. J. C* **23**, 311 (2002).
- [21] CMS Collaboration, CMS-PAS-EXO-15-004; ATLAS Collaboration, ATLAS-CONF-2015-081.

- [22] S. Fichet, G. von Gersdorff, C. Royon, *Phys. Rev. D* **93**, 075031 (2016); *Phys. Rev. Lett.* **116**, 231801 (2016) [arXiv:1601.01712 [hep-ph]].
- [23] S. Fichet *et al.*, *Phys. Rev. D* **89**, 114004 (2014); S. Fichet *et al.*, *J. High Energy Phys.* **1502**, 165 (2015).
- [24] M. Boonekamp *et al.*, arXiv:1102.2531 [hp-ph]; M. Boonekamp, V. Juranek, O. Kepka, C. Royon, arXiv:0903.3861 [hep-ph].
- [25] O. Kepka, C. Royon, *Phys. Rev. D* **78**, 073005 (2008).
- [26] G. Belanger, F. Boudjema, *Phys. Lett. B* **288**, 201 (1992).
- [27] G. Abbiendi *et al.* [OPAL Collaboration], *Phys. Rev. D* **70**, 032005 (2004) [arXiv:hep-ex/0402021].
- [28] CMS Collaboration, *J. High Energy Phys.* **1307**, 116 (2013); D0 Collaboration, *Phys. Rev. D* **88**, 012005 (2013).
- [29] E. Chapon, O. Kepka, C. Royon, *Phys. Rev. D* **81**, 074003 (2010); J. de Favereau *et al.*, arXiv:0908.2020 [hep-ph];
- [30] S. Fichet, G. von Gersdorff, *J. High Energy Phys.* **1403**, 102 (2014) [arXiv:1311.6815 [hp-ph]]; R.S. Gupta, *Phys. Rev. D* **85**, 014006 (2012).
- [31] L. Randall, R. Sundrum, *Phys. Rev. Lett.* **83**, 3370 (1999).
- [32] ATLAS Collaboration, ATL-PHYS-PUB-2013-009; *JINST* **3**, S08003 (2008).
- [33] J. Monk, A. Pilkington, *Comput. Phys. Commun.* **175**, 232 (2006); V.A. Khoze, A.D. Martin, M.G. Ryskin, *Eur. Phys. J. C* **55**, 363 (2008).
- [34] T. Sjostrand, S. Mrenna, P.Z. Skands, *Comput. Phys. Commun.* **178**, 852 (2008).
- [35] L.A. Harland-Lang, V.A. Khoze, M.G. Ryskin, *J. High Energy Phys.* **1603**, 182 (2016); A.D. Martin, M.G. Ryskin, *J. Phys. G* **43**, 04LT02 (2016).